Radiation Physics and Chemistry 185 (2021) 109513

Contents lists available at ScienceDirect

Radiation Physics and Chemistry

journal homepage: www.elsevier.com/locate/radphyschem

Additional radiation sources in a treatment and control room of medical linear accelerators

Adam Konefał [a,*], Marcin Bieniasiewicz [b], Jacek Wendykier [c], Sebastian Adamczyk [d], Aleksandra Wrońska [e]

[a] Institute of Physics, University of Silesia in Katowice, Katowice, Poland
[b] Radiotherapy Center, Department of Medical Physics, Multidisciplinary Hospital Gorzów Wielkopolski, Poland
[c] Maria Sklodowska-Curie National Research Institute of Oncology, Gliwice Branch, Radiotherapy Planning Department, Gliwice, Poland
[d] IntraOp Medical, Sunnyvale, USA
[e] Marian Smoluchowski Institute of Physics, Jagiellonian University, Kraków, Poland

ARTICLE INFO

Keywords:
Gamma-ray spectroscopy
Induced radioactivity
Neutrons
Radioactive decays
Prompt gamma rays

ABSTRACT

Typical medical linear accelerators generating high-energy photon beams used in radiotherapy are a source of neutrons and induced radioactivity undesirable mainly in radiological protection of medical staff but also for treatment of patients. The main source of the secondary radiation are massive components of an accelerator head. The purpose of this work was to study additional sources of gamma rays and neutrons in the treatment and control rooms for the Elekta accelerator. Identification of radioisotopes induced in several examined objects used and stored in the treatment room, and measurements of the spectrum of gamma rays originated in the treatment room door or travelling through it were carried out using a gamma–ray spectroscopy technique with an HPGe detector. Additionally, identification of neutron field was performed in the control room. In total, five nuclear reactions and five radioisotopes Mn-56, Sb-122, Fe-59, Li-7 and Al-28 were identified basing on gamma rays from the radioactive decays in the 20 cm × 20 cm electron applicator enabling collimation of the therapeutic electron beam, a Wood's alloy tray used as an additional shield against radiation, a special drawer for placing additional radiation shields, and a brick used to shield electronic modules of supporting equipment. Similarly, five nuclear reactions were also observed registering prompt gamma rays in the control room. The dominating nuclear reaction was the neutron capture. Moreover, the reactions induced by neutrons in the germanium crystal of the used HPGe detector confirmed the presence of neutrons in the control room.

1. Introduction

Presently, linear medical accelerators are widely used in radiotherapy. They provide various techniques of irradiation in photon modes as well as with electron beams (Diwanji et al., 2017; Gomez-Millan et al., 2013; Teoh et al., 2011). High-energy therapeutic beams can induce photonuclear reactions (γ,n) (Ma et al., 2002; Konefał et al., 2005; Hosseinzadeh et al., 2018; Wang et al., 2007), in which neutrons with a wide energy range (Tajiki et al., 2020) and various radioisotopes disintegrating by the EC and β^+ decay (Vega-Carrillo et al., 2011, 2015; Konefał et al., 2008a, 2008b; Soto-Bernal et al., 2017) may be formed. These neutrons contaminate the therapeutic beams. They can also induce further nuclear reactions ((n,γ), (n,n') etc.), resulting in the formation of neutron excess radioisotopes that decay mainly via β^-. This is especially important in terms of thermal and resonant energy. The main sources of neutrons are massive components of an accelerator head, such as collimators, targets and flattening filters (Mao et al., 1997). Radioisotopes may arise not only in the construction materials of the accelerator, but also in all objects in the treatment room, e.g. in wedges, individual shields, electron applicators. The source of radiation may also be the patient's body itself, including such items as cardiological devices, bioprostheses, etc. implemented in it (Konefał et al., 2020).

Some of the objects activated in the treatment room can be moved to an control room, becoming an undesirable source of radiation for technicians, physicists and physicians while these items in the treatment room are a source of an additional dose only for staff preparing a patient for irradiation. The door to the treatment room can also be a significant

* Corresponding author.
E-mail address: akonefal@us.edu.pl (A. Konefał).

https://doi.org/10.1016/j.radphyschem.2021.109513
Received 31 December 2020; Received in revised form 7 March 2021; Accepted 12 April 2021
Available online 16 April 2021
0969-806X/

source of unwanted radiation in the control room, as shown in (Konefał et al., 2016). In addition, a weak neutron field may appear in the control room during high-energy photon beam treatment. The aim of the study was to investigate additional sources of gamma radiation and neutrons in the room for radiotherapy and in the Elekta accelerator control room at the Oncology Center in Opole. The presented study is of particular importance for the radiation protection of hospital staff.

2. Materials and methods

The main measurement technique used in this work was gamma-ray spectroscopy. In the first stage of the research, several objects from the treatment room were examined. Immediately after the emission of the therapeutic X-ray beam of 18 MV generated by the Elekta medical linac (9000 monitor units, radiation field of 10 cm × 10 cm at 100 cm on the surface of a plastic phantom), the objects were moved to a different location outside the treatment room, where the energy spectra of gamma radiation emitted by these objects were recorded with the ORTEC detection system for field spectroscopy. It consisted of a high purity germanium (HPGe) detector connected to a computer operated from a PC. The detector operation was handled by the GammaVision software by PerkinElmer Instruments. The following objects were included in the measurements: an 20 cm × 20 cm electron applicator enabling collimation of the therapeutic electron beam, a Wood's alloy tray used as an additional shield against radiation, a special drawer for placing additional radiation shields, and a brick used to shield electronic modules of supporting equipment (Fig. 1).). When not in use, these items are often stored in the control room, becoming an undesirable source of radiation for hospital staff, mainly for technicians operating the accelerator.

In the second stage of the work, measurements of gamma-ray energy spectra were performed in two places (Fig. 2) in the accelerator control room during emission of 18 MV X-ray beams. The first location was in the vicinity of the door of the treatment room. The purpose of this measurement was to register the energy spectrum of gamma rays coming out of the door. The second measurement location was at the operator station, 2 m from the center of the door behind the wall separating the accelerator control room from the maze. The main purpose of this measurement was to study the neutron field in the control room.

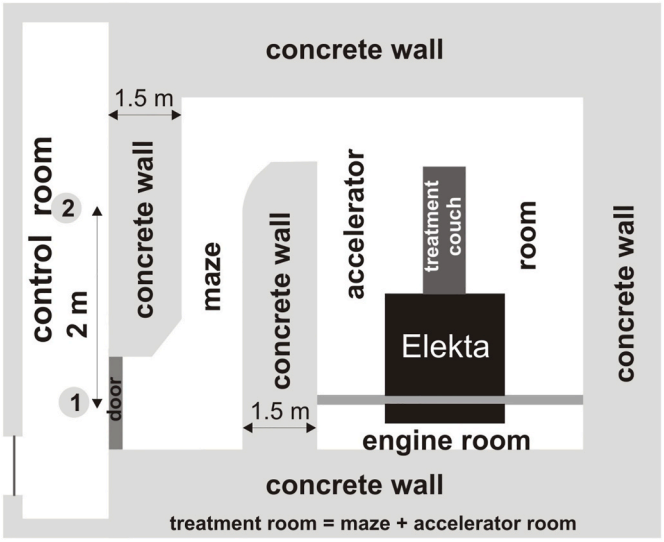

Fig. 2. The measuring places in the control room of the accelerator Elekta.

a. Calibration of the HPGe detector

Energy calibration (Fig. 3) was performed using a commercial ^{152}Eu

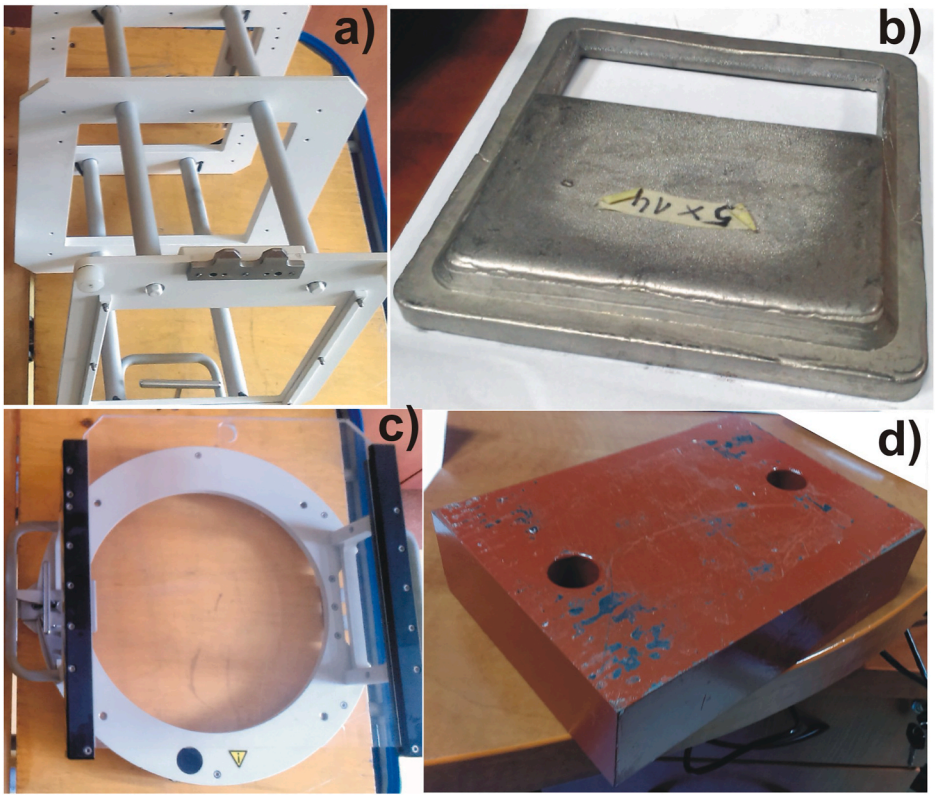

Fig. 1. A view of the objects investigated in this work. (a) The 20 cm × 20 cm electron applicator for therapeutic electron beam collimation, (b) the Wood's alloy tray used as an additional radiation shield, (c) the special drawer for placing additional radiation shields, (d) the brick for shielding various electronic parts of the accelerator.

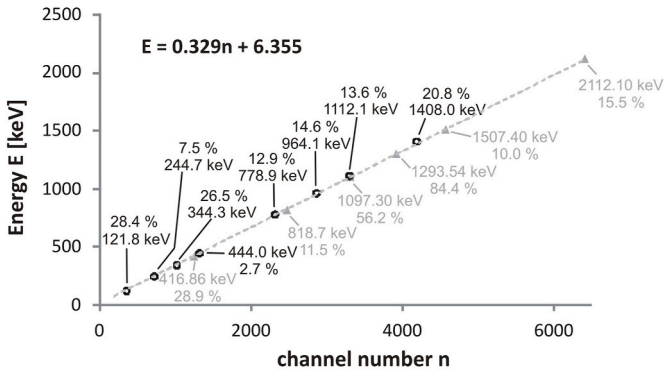

Fig. 3. Energy calibration curve determined using a commercial radiation source of ^{152}Eu and verified with the nuclear isomer of indium ^{116m}In at one of the measurement places. The points associated with the decays of ^{152}Eu (black circles) and ^{116m}In (gray triangles) are marked with gamma-ray energy values in keV and emission intensity in %. Indium-116m was produced by neutron activation of a natural indium foil near the Elekta accelerator head while emitting 18 MV X-ray beams.

radiation source at the nuclear physics laboratory of the University of Silesia in Katowice. The detection system used was relatively small and therefore portable. On the measuring stand, the energy calibration was verified with the use of the nuclear isomer of indium ^{116m}In originating from the simple neutron capture reaction ^{115}In(n,γ).

The efficiency calibration was also done using of ^{152}Eu. The detection efficiency ε (in %) can be expressed by the following equation (1):

$$\epsilon(E) = \frac{100 \cdot N_d(E)}{A_{CS} \cdot I(E)}, \quad (1)$$

where.

A_{CS} – the activity of the radiation source ^{152}Eu located on the surface of the detector shield (Fig. 4)

$N_d(E)$ – events collected in the photopeak (a net area) at energy E per unit of time in the calibration measurement.

I(E) – emission intensity of the gamma-rays forming the photopeak at E (taken from the Table of Isotopes (Firestone, 1996)).

The detection efficiency defined in eq. (1) was not used to determine the absolute activity of the identified radioisotopes due to differences in the size and shape of the calibration source and the tested objects. It was only used to determine the relative intensities of the photopeaks, which verified the assignment of parent radioisotopes to them (see Equation (3)). The applied ^{152}Eu calibration source with linear dimensions of 0.1 mm, enclosed in a plastic cylindrical capsule, was placed on the upper surface of the HPGe detector cover in evenly distributed positions as shown in Fig. 4. The mean net areas of the photopeaks, averaged for all measuring positions of the source were taken for the determination of the detection efficiency. In order to determine the detection efficiency, the average net area of the photopeaks, averaged for all source measurement positions, was adopted.

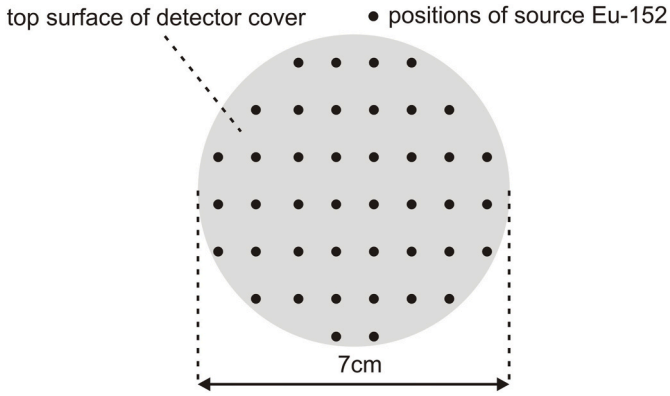

Fig. 4. The grid of ^{152}Eu calibration source positions on the upper surface of the HPGe-detector cover. Each black circle represents one location. The distances between the locations were constant.

The summing effect that can be observed in the efficiency curve, especially in the low and medium energy range, was corrected by Monte Carlo simulation (code GEANT4). The net area of each photopeak was obtained from a Gaussian fit after subtracting the background modeled with a polynomial. The efficiency-corrected relative intensity $R'(E_1, E_2)$ of two photopeaks at energies E_1 and E_2 can be described by the following formula (2):

$$R'(E_1, E_2) = \frac{N_d'(E_1) \; n \; W(E_1)}{N_d'(E_2) \; n \; W(E_2)} \quad (2)$$

where.

$N_d'(E_i)$ - events collected in a photopeak at energy E_i in the measurement with an activated object.

$W(E_i) = 100 \cdot \varepsilon(E_i)^{-1}$ is the inverse of the detection efficiency ε at energy E_i, multiplied by 100 and it can be called as the efficiency correction. The dependence between W and energy E of gamma rays is presented in Fig. 5.

If two photopeaks are produced in the decay of the same radioisotope, their efficiency-corrected relative intensity $R'(E_1, E_2)$ is expected to match the literature value $R(E_1, E_2)$:

$$R'(E_1, E_2) \approx R(E_1, E_2) = \frac{I(E_1)}{I(E_2)}, \quad (3)$$

where $I(E_1)$ and $I(E_2)$ are emission intensities of the gamma-rays forming the photopeaks at E_1 and E_2, respectively, read out from the Table of Isotopes (Firestone, 1996).

b. Registration of gamma-ray energy spectra

Each activated object, after removing it from the treatment room, was placed on the table with the HPGe detector, most often in the control room or in adjacent rooms where, apart from the activated objects, there was no other sources of radiation, obviously excluding natural radioactive isotopes. All these items contacted the upper surface of the germanium crystal cover to maximize the geometrical acceptance and thus the number of recorded events. The single spectrum acquisition time was 900 s. The Table of Isotopes edited by Firestone was used to analyze the measured spectra (Firestone, 1996). The database for gamma-ray neutron activation analysis, developed by the International

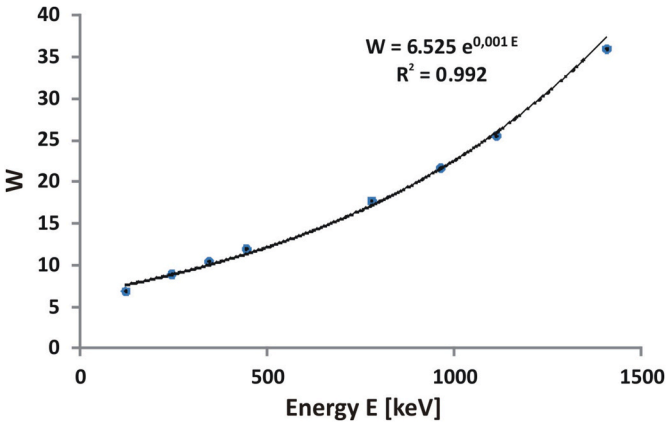

Fig. 5. The efficiency correction as a function of energy E of gamma rays, determined with the use of the commercial radiation source ^{152}Eu with activity of 27.92 kBq (the estimated value based on the activity at the time of manufacture).

Atomic Energy Agency, was also used (Database for Prompt Gamma-Ray Neutron Activation Analysis).

c. Method of the neutron field measurements

The spectroscopy of gamma rays stemming from the neutron capture reactions in the germanium crystal of the HPGe detector was used as a method of identifying weak neutron fields. The use of this method was possible due to the relatively low background of natural radiation, additionally reduced by the thick concrete walls surrounding the control room. In addition, radiotherapy centers usually do not have specialized equipment for measuring the neutron field, unlike germanium detectors, which are currently stocked in medical laboratories. We wanted to show that neutron identification probably does not require any dedicated neutron detector. The list of nuclear reactions with the energies of the accompanying gamma rays used to identify the neutron field and the suitable sections from the Brookhaven National Laboratory's Evaluated Nuclear Data Files (ENDF) are presented in Table 1.

Nuclear reactions used to identify neutron fields are characterized by strong resonances. The $^{73}Ge(n,\gamma_p)^{74}Ge$ reaction looks particularly favorably due to the three resonances above 1000 b occurring at energies below 1 eV, as well as the relatively high cross section of thermal neutrons.

3. Results and discussion

3.1. Gamma-ray spectroscopy for the objects activated inside the treatment room

The energy spectra of gamma rays emitted from the objects activated in the treatment room, registered immediately after activation, are shown in Fig. 6a – d.

All four spectra are quite similar. In three cases the radioisotope of manganese Mn-56 with a relatively short half – life of 2.57 h, contributing three photopeaks to the spectrum at 846.78 keV, 1810.77 keV and 2113.12 keV was identified. This radioisotope originates from the simple capture reaction $^{55}Mn(n,\gamma)^{56}Mn$. Mn-55 is the only natural isotope of manganese. This element is a component of stainless steel used commonly in electronics. Probably it is present in the pressure sensors located on the bottom side of the electron applicator and the drawer. In case of the brick, manganese improves mechanical properties of the alloy.

The radioisotope of antimony Sb-122 with a half – life of 2.7 d was identified in the electron applicator via its photopeak at 564.12 keV. This radioisotope originates from the simple capture reaction $^{121}Sb(n,\gamma)^{122}Sb$. The isotope Sb-121 has the abundance of 57.36%, higher than that of the second stable isotope of antimony Sb-123 (42.64%) which would change into Sb-124 in the (n,γ) reaction. Antimony is added to alloys to improve their hardness.

Furthermore, the radioisotope of iron Fe-59 generating two photopeaks at 1099.25 keV and at 1291.6 keV was identified in the tray made of Wood's alloy. This radioisotope originates from the simple capture reaction $^{58}Fe(n,\gamma)^{59}Fe$. The isotope Fe-58 has a relatively small abundance of 0.28%. The pure Wood's alloy should not contain Fe-58. Probably the iron got into the alloy from a vessel in which the alloy was heated. The other stable isotopes of iron with larger abundance change into stable isotopes in neutron-induced reactions or into long-lived radioisotopes and therefore gamma rays from their decays do not yield any noticeable contribution to the spectrum.

Table 1
The list of nuclear reactions, energies of gamma rays used for the identification of the neutron field and cross sections for the nuclear reactions occurring in the Ge crystal. γ_p - prompt-gamma rays from nuclear reactions occurring in the Ge crystal, γ_d – gamma rays from decays of produced nuclear isomers of germanium.

Nuclear reaction	Gamma-ray energy in keV	Cross section of reaction σ_{ther} at thermal energies and highest resonance
$^{70}Ge(n,\gamma_p)^{71m}Ge \rightarrow ^{71}Ge + \gamma_d$	**198.4**	σ_{ther} = 2.9 b 76.1 b at 1.12 keV 265.1 b at 1.47 keV 180.3 b at 1.94 keV 145.3 b at 3.14 keV 155.1 b at 4.23 keV 19.6 b at 4.38 keV 59.4 b at 4.51 keV 22.7 b at 4.94 keV
$^{73}Ge(n,\gamma_p)^{74}Ge$	**595.9, 867.9, 1204.2**	σ_{ther} = 14.4 b 1222.9 b at 102 eV 1804.4 b at 204 eV 1089.4 b at 225 eV 920.5 b at 321 eV 417.1 b at 332 eV 525.2 b at 367 eV 718.2 b at 408 eV 174.3 b at 490 eV 408.1 b at 516 eV 458.3 b at 557 eV 265.6 b at 668 eV 400.1 b at 919 eV
$^{74}Ge(n,\gamma_p)^{75m}Ge \rightarrow ^{75}Ge + \gamma_d$	**139.8**	σ_{ther} = 0.4 b 18.1 b at 2.85 keV 134.0 b at 3.04 keV 119.4 b at 4.17 keV

3.2. Gamma – ray spectroscopy in the control room

Two important problems motivated the undertaken measurements in the control rooms. The first is the gamma – ray production in simple capture reactions (n,γ) and the possible activation of materials in the door of the treatment room. The second is a possibility of the neutron penetration through this door and consequently the appearance of a slight neutron field in the control room. That field should be detected.

The energy range of the detection system has been extended to include measurements near the door of the treatment room, as the energy of gamma radiation generated in the door can reach almost 10 MeV. The increase of the energy range was related to a deterioration of the energy resolution due to coarser binning. After this change the FWHM of the 1332.5 keV peak of Co-60 was approximately 9 keV while for the remaining measurements it was 2.8 keV. The gamma – ray energy spectra presented in Fig. 7 were registered during emission of the 18 MV X-ray beam.

The door to the treatment room had a special construction i.e. most of used materials were deprived of metals except for aluminum components as a handle and screws. The latter is visible in the obtained spectrum via the appearance of two peaks at 1778.9 keV and at 7724.0 keV (Fig. 7a). This first one comes from the gamma transition in the excited nuclei of Si-28 originating from the β^- decay of Al-28 resulting from the simple capture reaction $^{27}Al(n,\gamma)Al^{28}$. The prompt gamma rays emitted in this reaction have an energy of 7724.0 keV and they contribute to the spectrum measured close to the treatment room door. The peaks corresponding to 5975.9 keV, 6485.9 keV, 6706.0 keV, 6985.4 keV, 7214.4 keV and 7491.5 keV are the prompt gamma rays originating from the simple capture reaction $^{59}Co(n,\gamma)^{60}Co$. However, this reaction did not occur in the door but in the materials (alloys) of the magnetic system steering the electrons onto the target. The evidence supporting this statement was presented in one of our previous work [12], where it was shown that the lines from the Co-60 decay were present in the spectrum measured in the vicinity of the head of the Elekta linac. These photopeaks are absent in the Fig. 7b because the gamma - rays are absorbed in the maze walls separating the treatment from the control room. In the reaction of neutrons with Co-59 the lower energy gamma rays are also produced. However, they are also absorbed before they can reach the detector. Therefore, their contribution to the spectrum is not visible. In the walls, the floor, the concrete ceiling as well as

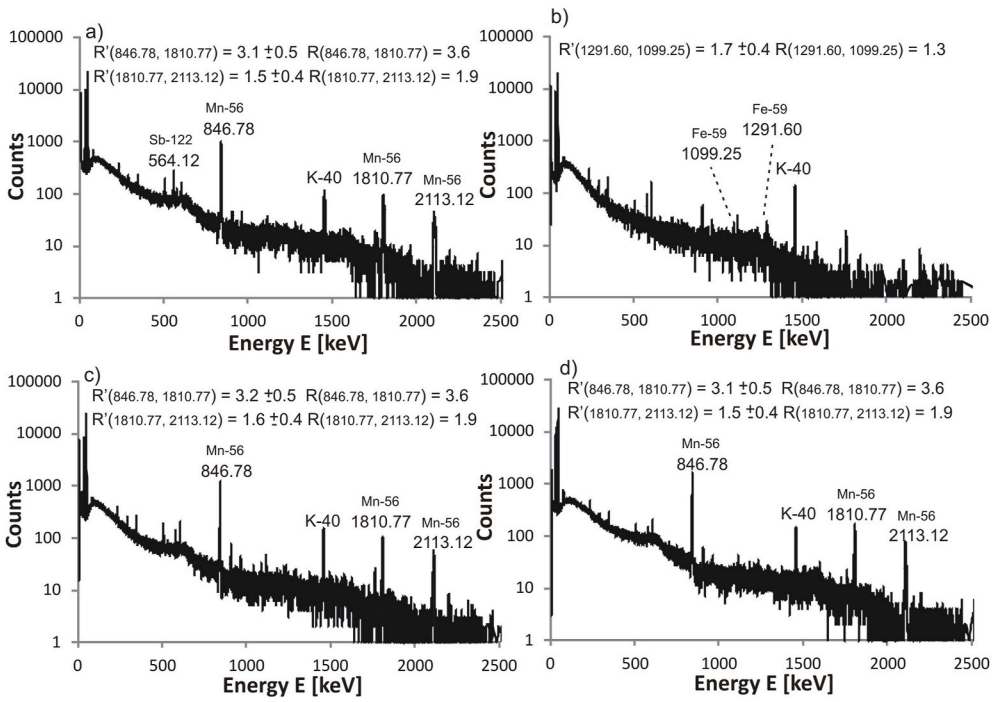

Fig. 6. The energy spectra with the visible gamma rays emitted by the activated objects. The spectra were registered directly after the objects were removed from the treatment room, after the 18 MV X-ray therapeutic beam emission. (a) The electron applicator, (b) the Wood's alloy tray, (c) the drawer, (d) the brick. The peaks from decays of radioisotopes produced in the objects are labeled with the radioisotope name and energy of a peak. Additionally, the peak from K-40 was denoted. Its intensity comparable to that for induced radioisotopes is the evidence for the slight activation. The remaining visible peaks come from natural radioisotopes. The value of R' close to R is the additional evidence for reliability of the identification of the radioisotopes induced in the considered objects.

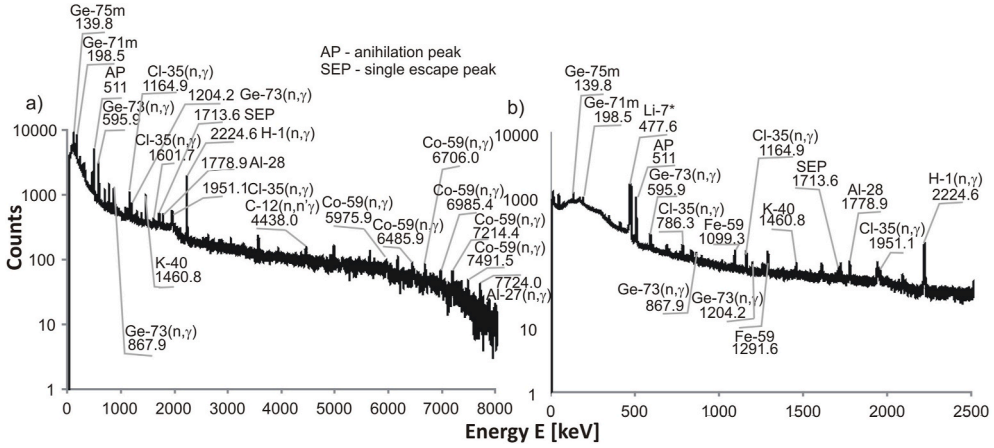

Fig. 7. The gamma - ray energy spectra registered in the control room during emission of the 18 MV X-ray beam a) close to the treatment room door b) and in the operator station at 2 m from the door center (see Fig. 2). The time of each measurement was 900 s.

in the hydrocarbon door, the reactions between the neutron field and the protons of hydrogen can occur. The evidence of this is a strong peak at 2224.6 keV formed by the gamma rays stemming from the reaction $^{1}H(n,\gamma)^{2}H$. This reaction occurs for slowed down neutrons and it is characterized by a relatively large cross section (see Table 3). The result of inelastic scattering of neutrons by the carbon nuclei is the emission of the 4438.0 keV prompt gamma rays. As the treatment room door was the only object containing large amount of carbon in the vicinity of the detector, the signal must have come from the door. The simple capture reaction $^{35}Cl(n,\gamma)^{36}Cl$ was also identified. It is represented by two photopeaks at 1164.9 keV and at 1951.1 keV in Fig. 7a. Third photopeak at 786.3 keV is only visible in Fig. 7b. The source of chlorine in the surroundings of the treatment room door is the PVC flooring. The radioisotopes of Fe-59 and Li-7 were identified in the measurement performed in the operator station. This first one originates from the reaction $^{58}Fe(n,\gamma)^{59}Fe$ followed by β^- decay with the emission of gamma rays of 1099.25 keV and 1291.6 keV. All together, the prompt gamma rays from this reaction have more than ten different energies, but small intensities hinder their observation. The sources of iron in the operator station are the stainless steel parts of chairs, tables and lockers. The radioisotope Li-7 was produced in the neutron-induced reaction with B-10: $^{10}B(n,\alpha)^{7}Li^{*}$ followed by a gamma decay with the emission of gamma rays of 477.6 keV visible in Fig. 7b. Boron is added to concrete walls to improve absorption of neutrons. The spectrum shown in Fig. 7b was registered for the therapeutic beam directed to the wall separating the accelerator room from the maze i.e. for the gantry setting of 90°. However, the same peaks with almost unchanged intensities appeared for gantry operated at 0°.

The remaining peaks visible in the spectrum recorded near the treatment room door are evidence of the presence of neutrons in the control room, as they are a result of interactions between neutrons and nuclei of germanium in the HPGe detector. In the Ge crystal the simple capture reaction with Ge-73 occurs. The detailed equation of this reaction is as follows: $^{73}Ge(n,\gamma)^{74}Ge$ with the prompt gamma rays at energies of 595.9 keV, 867.9 keV and 1204.2 keV. The photopeaks at these energies are also present in the spectrum measured in the operator station.

In germanium, the neutron-induced reaction with Ge-74, $^{74}Ge(n,\gamma)^{75}Ge$ also occurs. However, the prompt gamma – rays from these reactions did not give a visible contribution to the spectra measured in the control room. Moreover, this reaction can also lead to the excited metastable state of Ge-75m disintegrating to the ground state of Ge-75 by the emission of gamma rays at 139.8 keV forming the photopeaks present in both spectra measured in the control room (Fig. 7a and b). The analogous simple capture reaction was observed for Ge-70 in which the nuclear isomer Ge-71m was induced. Its deexcitation via the emission of gamma rays of 198.4 keV leads to the ground state of Ge-71.

In addition, dose measurements with a calibrated radiometer were carried out in the vicinity of the considered objects immediately after their activation and near the door of the treatment room and at the operator's station during the emission of the 18 MV X-ray beam. The maximum dose rate was measured on the surface of the treatment room door. However, it was relatively small and did not exceed 40 μS v per hour, measured with a calibrated radiometer EKO-C by Polon-Ekolab. This dose rate is too low to produce any direct biological effect. However, in line with ALARA's policy, radiation at workplaces should be kept to a minimum. The lowest possible level of radiation in a radiotherapy room can be achieved by implementing several practical solutions. First of all, as far as possible, all items in which longer-lived radioisotopes are produced should be removed from the treatment room. On the other hand, the problem of short-lived radionuclides, such as, for example, Al-28, can be solved by introducing a few-minute break between the end of the therapeutic beam emission and entering the room with the accelerator. In addition, it is worth monitoring the dose rate continuously in the accelerator room in the areas where staff are present and, if necessary and possible, *e.g.* to use boron shields to reduce the field of thermal neutrons. If possible, while cultivating the idea of ALARA, it is also worth avoiding a longer stay in direct proximity to the accelerator head and its disassembled components used to form the radiation field, especially after longer beam emission. Moreover, a workplace should not be installed in the control room near the door to the treatment room.

4. Summary

The radiation sources studied in this work were characterized by low activities, as evidenced by the method used. The gamma - ray spectroscopy is used to study low activity materials which do not generate higher dose rates. As mentioned, the highest recorded dose rate occurred on the surface of the treatment room door and it was relatively small, not exceeding 40 μSv per hour. The dose rate at this level not only does not exceed, but does not even come close to the dose limits specified in the Nuclear Law. In order to better understand the level of radiation emitted by the tested objects, it is worth considering the potential situation with the dose rate of 40 μSv/h. Suppose the technicians operating the accelerator work 8 h a day for 5 days a week. In addition, suppose a technician works 50 weeks a year. Of course, only a certain fraction of the time is spent in the vicinity of the additional radiation sources considered. For the presented considerations, let us assume that only for about 1/5 of the working time the technician is exposed to additional radiation generating a dose rate of 40 μSv/h. Under such assumptions, the accelerator operator receives a dose of about 9.5 mSv from additional radiation sources within a year, while the limit dose defined in the Nuclear Law is 20 mSv/year. Thus, the contemplated dose reduction from additional radiation sources is by no means a requirement that must be met in order not to exceed the dose limits specified in the Nuclear Law. The proposed solutions allow only to minimize the dose, adhering to the idea of ALARA.

The detailed information about the identified radioisotopes and nuclear reactions is summarized in Tables 2 and 3. The main sources of the presented data including half – lives of radioisotopes, emission intensities of gamma – rays and cross sections of nuclear reactions were the Table of Isotopes by Firestone, the Evaluated Nuclear Data Files (ENDF) by Brookhaven National Laboratory and the Database for Prompt Gamma-Ray Neutron Activation Analysis by the International Atomic Energy Agency. In total, five nuclear reactions and five radioisotopes (Table 2) were identified basing on the spectroscopy of gamma rays from the radioactive decays. Similarly, five nuclear reactions (Table 3) besides those in the Ge crystal were also observed by registering prompt gamma rays. The nuclear reactions were mainly the simple neutron capture.

Table 2
Characteristics of the radioisotopes identified via their radioactive decays.

Nuclear reaction and abundance of mother isotope in %	Cross section of reaction σ_{ther} at thermal energies and highest resonances	Produced radioisotope	Radioactive decay and its half - life	Energy of emitted gamma ray from decay in keV and its emission intensity in %
$^{55}Mn(n,\gamma)$ (100)	$\sigma_{ther} = 13.2$ b 149 b at 1660 eV	Mn-56	β-, 2.57 h	846.8 98.9 1810.8 27.2 2113.1 14.3
$^{121}Sb(n,\gamma)$ (57.36)	$\sigma_{ther} = 20$ b 5370 b at 15.5 eV 4720 b at 6.24 eV	Sb-122	β-, 2.7 days	564.1 69
$^{58}Fe(n,\gamma)$ (0.28)	$\sigma_{ther} = 1.15$ b 391 b at 359 keV	Fe-59	β-, 43.5 days	1099.3 56.5 1291.6 43.2
$^{10}B(n,\alpha)$ (19.9)	$\sigma_{ther} = 36000$ b	Li-7 in an excited state	γ, 73 fs	477.6 10.52
$^{27}Al(n,\gamma)$ (100)	$\sigma_{ther} = 0.23$ b 4.69 b at 5.9 keV	Al-28	β-, 2.24 min.	1778.9100

Table 3
Characteristics of the radioisotopes identified basing on the associated prompt gamma - rays.

Nuclear reaction and abundance of mother isotope in %	Cross section of reaction σ_{ther} at thermal energies and highest resonances	Produced nucleus	Energy of emitted gamma ray in keV
$^{59}Co(n,\gamma)$ (100)	$\sigma_{ther} = 37.17$ b 863.1 b at 132 eV	Co-60	5975.9 6485.9 6706.0 6985.4 7214.4 7491.5
$^{35}Cl(n,\gamma)$ (75.77)	$\sigma_{ther} = 32.85$ b	Cl-36	786.3 1164.9 1601.7 1951.1
$^{12}C(n,n'\gamma)$ (98.9)	0.56 b at 8.11 MeV 0.58 b at 8.37 MeV	C-12	4438.0
$^{1}H(n,\gamma)$ (99.99)	$\sigma_{ther} = 0.333$ b	H-2	1713.6^{SEP} 2224.6
$^{27}Al(n,\gamma)$ (100)	$\sigma_{ther} = 0.23$ b 4.69 b at 5.9 keV	Al-28	7724.0

SEP – single escape peak.

5. Conclusions

The strongest radiation source responsible for a significant contribution to a dose obtained by the personnel. is of course the accelerator

head composed of massive materials as many works have shown. This problem was investigated in details and presented in (Polaczek-Grelik et al., 2010), for example. The various small accelerator accessories and objects like those considered in this study are often stored in the treatment room close to a treatment couch - the place where the staff members spend a lot of time performing their professional activities. In this case, the activated objects are a source of an additional dose to staff. Its value is strongly dependent on the time of emission of the high-energy X-ray beam, as well as the time of a person staying near objects. However, as shown, the doses from the additional radiation sources do not exceed the limits set out in the Nuclear Law. It is worth noting that the radioactivity of the objects can accumulate due to the relatively long half-lives of the induced radioisotopes. Therefore, it is recommended to avoid storing any items in the treatment room where activation occurs even outside the therapeutic beam, as the neutron field is almost constant and occurs throughout the accelerator room, as shown in (Biltekin et al., 2015; Bieniasiewicz et al., 2016). It is also not recommended to move any item from the treatment room to the control room.

The second problem is a radiation penetration through the treatment room door and producing radiation in that door. This problem can be successfully reduced by the use of the special door structure proposed in (Konefał et al., 2014).

The particularly important result is the confirmation of the presence of a slight neutron field in the operator station. There are many works describing the malfunctions of cardiac implantable electronic devices (CIED) after high-energy radiation exposure (Zaremba et al., 2015; Mollerus et al., 2014), where the slowed-down or fast neutrons were identified as a direct cause of those malfunctions. In microprocessors based on small voltage surges, located inside cardiac devices, a single neutron passing through random access memory (RAM) may leave voltage ripples or wakes, leading to the reprogramming of the software code or a change of bits from 1 to 0 and vice versa (Bisello et al., 2012). It is obvious that such malfunctions are an undesirable phenomenon. There are no legal regulations regarding the work of people with cardiac implantable electronic devices in conditions related to ionizing radiation. Only guidelines for cancer patients can be found in specialistic protocols. According to the Recommendations and Protocol for the Management of the CIED Patient Undergoing Radiation Therapy (Indik et al., 2017) and the European Heart Rhythm Association survey (Lenarczyk et al., 2017), a non–neutron-producing treatment to minimize the risk of the device reset is recommended.

Declaration of competing interest

The authors declare that they have no known competing financial interests or personal relationships that could have appeared to influence the work reported in this paper.

References

Bieniasiewicz, M., Konefał, A., Wendykier, J., Orlef, A., 2016. Measurements of thermal and resonance neutron fluence and induced radioactivity inside bunkers of medical linear accelerators in the center of oncology in Opole, Poland. Acta Phys. Pol. B 47 (3), 771–776.

Biltekin, F., Yeginer, M., Ozyigit, G., 2015. Investigating in-field and out-of-field neutron contamination in high-energy medical linear accelerators based on the treatment factors of field size, depth, beam modifiers, and beam type. Phys. Med. 31 (5), 517–523.

Bisello, D., Candeloria, A., Dzysiuk, N., Esposito, J., Mastinu, P., Mattiazzo, S., Prete, G., Silvestrina, L., Wyss, J., 2012. Neutron production targets for a new single event effects facility at the 70 MeV cyclotron of LNL-INFN. Physics Procedia 26, 284–293.

Database for Prompt Gamma-Ray Neutron Activation Analysis by the International Atomic Energy Agency. https://www-nds.iaea.org/pgaa/.

Diwanji, T.P., Mohindra, P., Vyfhuis, M., Snider, J.W., Kalavagunta, C., Mossahebi, S., Yu, J., Feigenberg, S., Badiyan, S.N., 2017. Advances in radiotherapy techniques and delivery for non-small cell lung cancer: benefits of intensity-modulated radiation therapy, proton therapy, and stereotactic body radiation therapy. Transl. Lung Cancer Res. 6 (2), 131–147.

Evaluated Nuclear Data Files (ENDF) by Brookhaven National Laboratory. http://www.nndc.bnl.gov/sigma/search.jsp.

Version 1.0. In: Firestone, R.B. (Ed.), 1996. Table of Isotopes, eighth ed. University of California, Lawrence Berkeley National Laboratory.

Gomez-Millan, J., Fernández, J.R., Carmona, J.A.M., 2013. Current status of IMRT in head and neck cancer. Rep. Practical Oncol. Radiother. 18, 371–375.

Hosseinzadeh, E., Banaee, N., Nedaie, H.A., 2018. Monte Carlo calculation of photo-neutron dose produced by circular cones at 18 MV photon beams. Rep. Practical Oncol. Radiother. 23, 39–46.

Indik, J.H., Gimbel, J.R., Abe, H., 2017. HRS expert consensus statement on magnetic resonance imaging and radiation exposure in patients with cardiovascular implantable electronic devices. Heart Rhythm 14, e97–e153.

Konefał, A., Polaczek-Grelik, K., Zipper, W., 2008b. Undesirable nuclear reactions and induced radioactivity as a result of the use of the high-energy therapeutic beams generated by medical linacs. Radiat. Protect. Dosim. 128 (2), 133–145.

Konefał, A., Blamek, S., Wrońska, A., Orlef, A., Sokół, M., Tajstra, M., Gąsior, M., 2020. Radioactivity induced in new-generation cardiac implantable electronic devices during high-energy X-ray irradiation. Appl. Radiat. Isot. 163, 109206.

Konefał, A., Dybek, M., Zipper, W., Łobodziec, W., Szczucka, K., 2005. Thermal and epithermal neutrons in the vicinity of the Primus Siemens biomedical accelerator. Nukleonika 50 (2), 73–81.

Konefał, A., Łaciak, M., Dawidowska, A., Osewski, W., 2014. Significant change in the construction of a door to a room with slowed down neutron field by means of commonly used inexpensive protective materials. Radiat. Protect. Dosim. 162 (3), 197–207.

Konefał, A., Orlef, A., Dybek, M., Maniakowski, Z., Polaczek-Grelik, K., Zipper, W., 2008a. Correlation between radioactivity induced inside the treatment room and the undesirable thermal/resonance neutron radiation produced by linac. Phys. Med. 24, 212–218.

Lenarczyk, R., Potpara, T.S., Haugaa, K.H., Deharo, J.C., Hernandez-Madrid, A., Pineda, M.C.E., Kiliszek, M., Dagres, N., 2017. Approach to cardio-oncologic patients with special focus on patients with cardiac implantable electronic devices planned for radiotherapy: results of the European Heart Rhythm Association survey. EP Europace 19, 1579–1584.

Ma, A., Awotwi-Pratt, J., Alghamdi, A., Alfuraih, A., Spyrou, N.M., 2002. Monte Carlo study of photoneutron production in the Varian Clinac 2100C linac. J. Radioanal. Nucl. Chem. 276, 119–123.

Mao, X.S., Kase, K.R., Liu, J.C., Nelson, W.R., Kleck, J.H., Johnsen, S., 1997. Neutron sources in the Varian Clinac 2100C/2300C medical accelerator calculated by the EGS4 code. Health Phys. 72, 524–529.

Mollerus, M., Naslund, L., Lipinski, M., Meyer, A., Libey, B., Dornfeld, K., 2014. Radiation tolerance of contemporary implantable cardioverter-defibrillators. J. Intervent. Card Electrophysiol. 39 (2), 171–175.

Polaczek-Grelik, K., Orlef, A., Dybek, M., Konefał, A., Zipper, W., 2010. Linear accelerator therapeutic dose - induced radioactivity dependence. Appl. Radiat. Isot. 68, 763–766.

Soto-Bernal, T.G., Baltazar-Raigosa, A., Medina-Castro, D., Vega-Carrillo, H.R., 2017. Neutron production during the interaction of monoenergetic electrons with a Tungsten foil in the radiotherapeutic energy range. Nucl. Instrum. Methods Phys. Res. A 868, 27–38.

Tajiki, S., Nedaie, H.A., Rahmani, F., 2020. A Monte Carlo study of neutron contamination in presence of circular cones during stereotactic radiotherapy with 18 MV photon beams. Biomedical Physics & Engineering Express 6 (3), 035016.

Teoh, M., Clark, C.H., Wood, K., Whitaker, S., Nisbet, A., 2011. Volumetric modulated arc therapy: a review of current literature and clinical use in practice. Br. J. Radiol. 84, 967–996.

Vega-Carrillo, H.R., Baltazar-Raigosa, A., 2011. Photoneutron spectra around an 18 MV linac. J. Radioanal. Nucl. Chem. 287, 323–327.

Vega-Carrillo, H.R., Leon-Martinez, H.A., Rivera-Perez, E., Benites-Rengifo, J.L., Gallego, E., Lorente, A., 2015. Induced radioisotopes in a linac treatment hall. Appl. Radiat. Isot. 102, 103–108.

Wang, Q.B., Masumoto, K., Bessho, K., Matsumura, H., Miura, T., Shibata, T., 2007. Evaluation of the radioactivity in concrete from accelerator facilities. J. Radioanal. Nucl. Chem. 273, 55–58.

Zaremba, T., Jakobsen, A.R., Søgaard, M., 2015. Risk of device malfunction in cancer patients with implantable cardiac device undergoing radiotherapy: a population-based cohort study. PACE - Pacing Clin Electrophysiol. 38 (3), 343–356.